Electronic Supplementary Material (ESI) for Environmental Science: Processes & Impacts.

Indirect photodegradation of the lampricides TFM and niclosamide

Megan B. McConville,[1] Stephen P. Mezyk,[2] and Christina K. Remucal[1,3]*

[1]Environmental Chemistry and Technology Program

University of Wisconsin – Madison

Madison, Wisconsin

[2]Department of Chemistry and Biochemistry

California State University – Long Beach

Long Beach, California

[3]Department of Civil and Environmental Engineering

University of Wisconsin – Madison

Madison, Wisconsin

Contents (31 pages): Figures S1 – S16, Tables S1 – S5, Scheme S1

* Corresponding author address: 660 N. Park St., Madison, WI 53705;
e-mail: remucal@wisc.edu; telephone: (608) 262-1820; fax: (608) 262-0454

Table of Contents

Section S1. Materials.

Acetonitrile (HPLC grade), methanol (HPLC grade), and formic acid (ACS, 88%) were purchased from Fisher Chemical. 3-Trifluoromethyl-4-nitrophenol (TFM; 99%) *para*-nitroanisole (PNA; ≥99%), deuterium chloride (DCl; 20 wt% in D_2O, 100.0 Atom % D), and sodium deuteroxide (NaOD; 30 wt% in D_2O, 99+ Atom % D) were purchased from Acros Organics. 2',5-Dichloro-4'-nitrosalicylanilide (niclosamide; NIC; ≥98%), 2-chloro-4-nitroaniline (99%), 2-chloro-4-nitrophenol (97%), 4-nitrocatechol (97%), 1,2,4-benzenetriol (4-hydroxycatechol; 99%), 5-chlorosalicylic acid (98%), 2-5-dihydroxybenzoic acid (gentisic acid; ≥98%), maleic acid (≥99%), trifluoroacetic acid (99%), terephthalic acid (TPA; 98%), hydroxy-terephthalic acid (hTPA; 97%), sodium phosphate dibasic (ACS, ≥99%), ammonium acetate (≥97%), sorbic acid (≥99%), *N.N*-dimethylaniline (DMA; 99%), 2,4,6-trimethylphenol (TMP; 98%), and deuterium oxide (D_2O; 99.9 Atom % D) were purchased from Sigma Aldrich Co., LLC. Pyridine (≥99%) was purchased from Alfa Aesar. Sodium borate (ultrapure grade) and boric acid (ACS) were purchased from Amresco. Furfuryl alcohol (FFA; 98%) was purchased from Alpha Aesar. Isopropyl alcohol (IPA; HPLC grade, 99.9%) and sodium bromide (NaBr; 99+%) was purchased from Fisher Scientific. Suwannee River fulvic acid II (SRFA II) and Pony Lake fulvic acid (PLFA) organic matter isolates were purchased from the International Humic Substances Society (IHSS). All other chemicals were analytical grade from common commercial sources. All chemicals were used as received.

Section S2. Watershed parameters, sample locations, and river chemical composition.

The general watershed characteristics of the five tributaries assessed in this study are provided in **Table S1**. This data was determined from the Great Lakes Hydrography Dataset,[1] the

2011 National Land Cover Database,[2] and the Great Lakes Aquatic Habitat Framework.[3] The watershed land use and sample locations are presented in **Figure S1**.

Table S1. Tributary length, order, watershed size, and watershed land use of the five Lake Michigan tributaries used throughout this study.

Parameter		Milwaukee River	Sheboygan River	Fox River	Menominee River	Manistique River	Reference(s)
Total stream length	(km)	923	494	7,019	4,383	1,356	1,3
Stream order	(-)	4	4	6	6	5	1,3
Watershed size	(km^2)	2,240	1,127	16,487	10,535	3,810	1,3
Watershed land use	(%)	urban 30.2%, forested 12.2%, agricultural 43.6%, wetland 12.3%	urban 10.0%, forested 10.2%, agricultural 63.9%, wetland 14.6%	urban 9.0%, forested 26.3%, agricultural 44.3%, wetland 19.3%	urban 4.0%, forested 55.1%, agricultural 4.5%, wetland 31.8%	urban 3.1%, forested 39.1%, agricultural 1.0%, wetland 48.6%	2

Figure S1. Sample locations and land use in the Lake Michigan watershed. Land use designation was assigned according to the 2011 National Land Cover Database.[2]

Parameters used to describe the general river chemical composition are included in **Table S2.** These parameters include: pH, alkalinity, dissolved organic carbon (DOC), inorganic carbon (IC), total carbon (TC), specific UV absorbance at 254 nm ($SUVA_{254}$; a proxy for aromaticity),[4–6] the E_2:E_3 ratio (absorbance at 254 divided by the absorbance at 365, which inversely correlates with molecular weight),[7] as well as primary anions and cations present in solution. The UV-visible absorption spectra of the river samples are presented in **Figure S2**.

Table S2. Water chemistry data for the five Lake Michigan tributaries.

Parameter			**Milwaukee River**	**Sheboygan River**	**Fox River**	**Menominee River**	**Manistique River**
pH		(-)	8.45	8.53	8.42	8.33	8.17
Alkalinity		mg-$CaCO_3$ L^{-1}	275.84 ± 0.54	280.45 ± 3.63	140.71 ± 2.41	104.74 ± 1.59	48.25 ± 1.54
DOC		mg-C L^{-1}	7.13 ± 0.12	7.50 ± 0.26	8.83 ± 0.00	11.63 ± 0.15	23.27 ± 0.15
IC		mg-C L^{-1}	63.20 ± 0.30	65.27 ± 0.06	33.13 ± 0.06	23.40 ± 0.00	9.94 ± 0.01
TC		mg-C L^{-1}	70.30 ± 0.20	72.80 ± 0.27	41.93 ± 0.06	35.03 ± 0.15	33.97 ± 0.21
$SUVA_{254}$		L mg-C^{-1} m^{-1}	3.96	3.77	2.52	3.74	4.15
E_2:E_3		(-)	6.45	6.36	8.25	5.95	4.72
anions	Cl^-	ppm	111.62	71.26	29.75	11.22	10.89
	NO_2^-	ppm	4.44	4.75	3.14	2.52	1.25
	NO_3^-	ppm	5.46	1.69	0.10	0.38	0.00
	SO_4^{2-}	ppm	32.32	28.91	24.82	16.31	12.83
cations	Ca	ppm	78.41	69.02	35.77	27.99	26.28
	Fe	ppm	ND	ND	ND	0.02 ± 0.00	0.43 ± 0.00
	K	ppm	3.09	3.99	2.44	1.31	0.23
	Mg	ppm	38.82	38.08	21.91	12.94	1.90
	Na	ppm	62.43	41.14	18.09	11.09	0.31

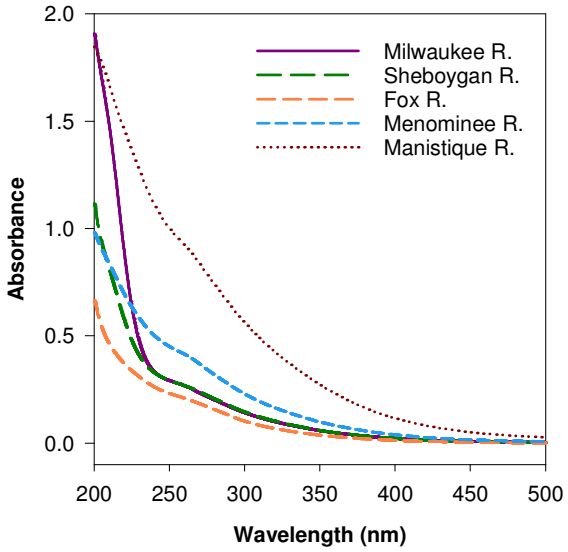

Figure S2. UV-visible absorption spectra of bulk samples collected from the five tributaries of Lake Michigan.

Parameters collected using an *in situ* YSI EXO sonde multimeter at the time of sample collection in the five river tributaries are included as **Table S3**. These parameters include: date, latitude, longitude, temperature, conductivity, optical dissolved oxygen (ODO), pH, the maximum depth, river turbidity, chlorophyll-a, fluorescent dissolved organic matter (fDOM), and barometric pressure.

Table S3. Average EXO sonde data recorded at the time of sample collection.

Parameter		**Milwaukee River**	**Sheboygan River**	**Fox River**	**Menominee River**	**Manistique River**
Date	(-)	7/29/2013	7/29/2013	7/30/2013	7/30/2013	7/31/2013
Latitude	°N	43.0550	43.7510	44.4590	45.1027	45.9710
Longitude	°W	-87.9050	-87.7250	-88.0685	-87.6289	-86.2430
Temperature	°C	20.2 ± 0.5	20.5 ± 0.7	21.7 ± 0.2	21.3 ± 0.0	17.3 ± 0.0
Conductivity	µS cm^{-1}	744.1 ± 8.4	670.7 ± 22.7	361.1 ±1.2	239.5 ± 0.1	117.7 ± 0.2
ODO	mg L^{-1}	7.88 ± 0.26	15.22 ± 1.25	13.56 ± 0.65	8.72 ± 0.01	7.58 ± 0.01
pH	(-)	8.27 ± 0.01	8.55 ± 0.05	9.18 ± 0.05	7.99 ± 0.01	7.09 ± 0.02
Max depth	m	2.79	0.20	1.24	0.16	0.74
Turbidity	FNU	8.0 ± 2.5	4.8 ± 0.5	55.5 ± 21.8	1.9 ± 0.5	7.7 ± 0.5
Chlorophyll-a	µg L^{-1}	2.60 ± 0.55	2.54 ± 0.31	27.99 ± 7.79	3.41 ± 0.07	7.97 ± 0.09
fDOM	QSU	92.8 ± 1.3	83.5 ± 6.2	48.9 ± 3.2	107.2 ± 0.0	164.0 ± 0.2
Barometric pressure	mm Hg	750.4 ± 0.1	750.6 ± 0.3	750.7 ± 0.1	749.4 ± 0.1	746.6 ± 0.1

Section S3. Irradiation sources.

Two different light sources were utilized during this study. Niclosamide photochemical experiments were generally performed in a Rayonet merry-go-round photoreactor equipped with sixteen 365 nm bulbs (Southern New England Ultraviolet Co. RPR-3500 Å; width at half-maximum = ± 9 nm; **Figure S3**).[8] The emitted irradiation from the 365 nm bulbs is within the spectrum of natural sunlight. Secondly, a 450 W Xe lamp (627NS, Newport Corporation) was utilized for most TFM and organic photoproduct photochemical experiments. The lamp was equipped with an Oriel Company 59450 filter to cut off light below 290 nm and was selected as it is similar to natural sunlight.

The spectra of the 365 nm bulbs and the xenon lamp were measured using a spectrophotometer (Model FLAME-S-UV-VIS-ES). The spectra were measured for each light source by holding the spectrophotometer perpendicular to the lamps at a distance far enough away from the lamp to not max out the detector, but close enough to generate a representative spectrum. The light intensity was quantified using a *p*-nitroanisole/pyridine actinometer using the revised quantum yield.[9] Two configurations were employed for TFM experiments; one slightly closer to the lamp (Xe-1) and one further from the lamp (Xe-2). The Xe-1 configuration was used for preliminary experiments, while the Xe-2 configuration was used in most experiments as it accommodates more test tubes. **Figure S3** shows the intensity of the 365 nm bulbs, as well as the two Xe lamp configurations. The apparent intensity of each configuration was calculated by summing the intensity values at each wavelength from 200-500 nm (i.e., the region where the two lampricides absorb light).[10] Xe-1 has an apparent intensity an order of magnitude greater than Xe-2; 1.98×10^{-4} and 2.02×10^{-5} mE cm^{-2} s^{-1}, respectively. In comparison, the apparent intensity of the 365 nm bulbs is 1.43×10^{-4} mE cm^{-2} s^{-1}.

Borosilicate test tubes were used in the Rayonet photoreactor as opposed to quartz test tubes used in the Xe lamp experiments. The spectra of light emitted from the 365 nm bulbs in borosilicate tubes and quartz test tubes are equivalent, as demonstrated in **Figure S4**.

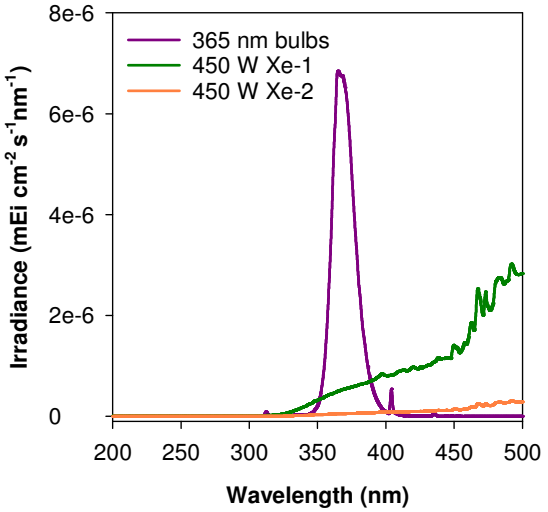

Figure S3. The intensity of the two light sources used in this study: 365 nm bulbs in a Rayonet photoreactor and two configurations using a 450 W Xe lamp equipped with an Oriel Company 59450 filter to cut off light below 290 nm.

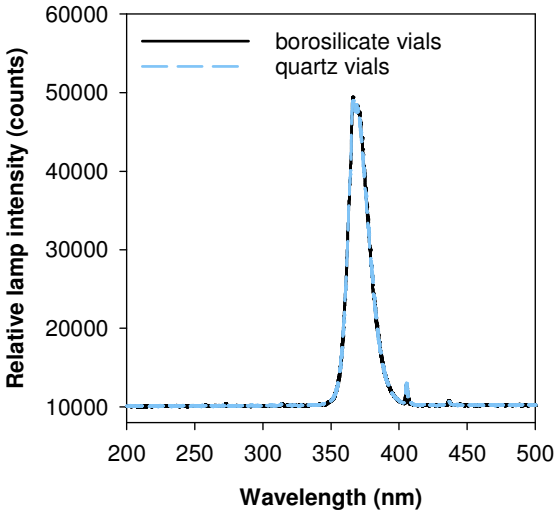

Figure S4. Representative light spectra from a Rayonet photoreactor equipped with 365 nm bulbs collected using a spectrophotometer within a borosilicate test tube and a quartz test tube.

Section S4. Calculations.

Steady state determination. The apparent steady state concentrations of singlet oxygen ($^1O_2$), triplet dissolved organic matter (^{3}DOM), and hydroxyl radical ($^{\bullet}$OH) were quantified in all five river water samples using known probe compounds. The $^1O_2$ steady state was quantified by monitoring the loss of FFA with time according to the following equations:[11–14]

$$\frac{d[FFA]}{dt} = -k_{FFA,\ ^1O_2} \cdot [FFA] \cdot [^1O_2]_{SS} \quad \text{(S1)}$$

$$[^1O_2]_{SS} = \frac{d(-\ln\left(\frac{[FFA_t]}{[FFA_0]}\right))}{dt} \cdot (k_{FFA,\ ^1O_2})^{-1} \quad \text{(S2)}$$

where the observed pseudo-first-order loss of FFA as a function of time is divided by the known bimolecular rate constant between FFA and $^1O_2$ ($k_{FFA,\ ^1O_2} = 1.0 \times 10^8$ M^{-1} s^{-1}).[15] Similarly, the ^{3}DOM steady state concentration was determined from the loss of TMP as a function of time according to the following equations:

$$\frac{d[TMP]}{dt} = -k_{TMP,\ ^3DOM} \cdot [TMP] \cdot [^3DOM]_{SS} \quad \text{(S3)}$$

$$[^3DOM]_{SS} = \frac{d(-\ln\left(\frac{[TMP_t]}{[TMP_0]}\right))}{dt} \cdot (k_{TMP,\ ^3DOM})^{-1} \quad \text{(S4)}$$

where the observed pseudo-first-order loss of TMP as a function of time is divided by the estimated bimolecular rate constant between TMP and ^{3}DOM ($k_{TMP,\ ^3DOM} = 2.6 \times 10^9$ M^{-1} s^{-1}).[14,16]

The steady state concentration of $^{\bullet}$OH is more challenging to determine due to the highly indiscriminate nature of its reaction with organic compounds.[17] The apparent steady state concentration was determined by monitoring the formation of hTPA upon the irradiation of TPA.[18,19] Monitoring the formation of hTPA is advantageous because the molecule is fluorescent, and thus can be detected at low concentrations. While an ideal probe molecule is resistant to direct photodegradation, hTPA is known to undergo direct photodegradation at wavelengths below 360

nm.[19] These experiments were conducted using 365 nm (± 9 nm) bulbs and thus the rate of direct photodegradation of hTPA was accounted for in Equation **S5** below. Additionally, •OH reacts with hTPA at a known rate ($k_{hTPA,\cdot OH}$ = 6.3 × 10^9 M^{-1} s^{-1}). Accounting for these aspects, the following previously published equation was employed:[19]

$$\frac{d[hTPA]}{dt} = (0.35 \cdot (k_{TPA,\cdot OH} \cdot [TPA] \cdot [^{\bullet}OH]_{SS})) - [hTPA] \cdot (k_{hTPA,\cdot OH} \cdot [^{\bullet}OH]_{SS} + k_{hTPA,direct}) \quad (S5)$$

where the first term (in blue) represents the loss of TPA by reaction with •OH as a function of time, and thus the formation of hTPA. This reaction is 35% efficient and is based on the known rate of reaction between TPA and •OH (i.e., $k_{TPA,\cdot OH}$ = 4.4 × 10^9 M^{-1} s^{-1}).[19] The second term (in red) accounts for the photodegradation of hTPA by •OH, and the final term (in black) accounts for the measured direct photodegradation of hTPA by exposure to the 365 nm bulbs. The steady state concentration of •OH was determined by solving the equation and minimizing the sum of squared error between the modeled data and the measured concentration of hTPA at each time interval.

Finally, the carbonate radical ($CO_3^{-\bullet}$) steady state concentration was calculated using the steady state concentration of •OH, the alkalinity of the sample, the standardized dissolved organic carbon content (6.8 mg-C L^{-1}), and the standardized pH (8.00) according to the following equation:[20,21]

$$[CO_3^{\cdot -}]_{SS} = \frac{k_{HCO_3^-,\cdot OH}[HCO_3^-][^{\bullet}OH]_{SS} + k_{CO_3^{2-},\cdot OH}[CO_3^{2-}][^{\bullet}OH]_{SS}}{k_{CO_3^{\cdot -},DOM}[TOC]} \quad (S6)$$

This equation assumes that $CO_3^{-\bullet}$ is only formed from the reaction of •OH and bicarbonate or carbonate,[11,21,22] and that the primary quencher of $CO_3^{-\bullet}$ is dissolved organic matter (DOM). The rates of reaction between the carbonate species and •OH are known (i.e., $k_{HCO_3^-,\cdot OH}$ = 8.5 × 10^6 M^{-1} s^{-1} and $k_{CO_3^{2-},\cdot OH}$ = 3.9 × 10^8 M^{-1} s^{-1}).[23] For these calculations, alkalinity was assumed to be the sum of [HCO_3^-] and two times the [CO_3^{2-}] in solution. Finally, the rate of reaction between $CO_3^{-\bullet}$

and DOM was estimated previously for DOM from a wastewater effluent wetland treatment cell (i.e., 3.7×10^2 (mg-C L^{-1})$^{-1}$ s^{-1}).[20]

Quencher efficiency. Calculations were performed to determine the ideal quencher concentration required to selectively quench each photochemically produced reactive intermediate (PPRI). IPA was used to quench $^{\bullet}OH$,[13] FFA was used to quench for $^1O_2$,[12] and sorbic acid was used to quench ^{3}DOM.[24,25] Utilizing the equations published by Bodhipaksha *et al.*,[21] we determined a range in quencher efficiency of each probe compound (**Table S4**). In brief, these equations account for the reaction between the PPRI (e.g., $^{\bullet}OH$) and the quencher (e.g., IPA), as well as the PPRI and the most prominent natural sink present in solution (i.e., DOM for $^{\bullet}OH$, H_2O for $^1O_2$, and dissolved O_2 for ^{3}DOM).

Table S4. Quencher concentration and the resulting estimated quencher efficiency for IPA, FFA, and sorbic acid. The values in ***bold italics*** refer to the concentrations we selected in our quencher experiments.

[DOC]	IPA added	Quenching efficiency (IPA)	FFA added	Quenching efficiency (FFA)	Sorbic acid added	Quenching efficiency (sorbic acid)
(mg-C L^{-1})	(mM)	(%)	(mM)	(%)	(mM)	(%)
6.8	4	97.57	1	28.57	1	84.21
6.8	10	99.01	***4***	***61.54***	2	91.43
6.8	***25***	***99.60***	10	80.00	***4***	***95.52***
6.8	100	99.90	40	94.12	7	97.39

As noted in **Table S4**, 25 mM IPA, 4 mM FFA, and 4 mM sorbic acid concentrations were selected for subsequent quencher experiments. The 25 mM IPA concentration was validated using a separate control experiment. In this experiment, the range of IPA concentrations referred to in **Table S4** (i.e., 4, 10, 25 and 100 mM) were added to solutions containing 10 µM niclosamide in 5 mM borate-buffered (pH 8) Milwaukee River water (DOC = 6.8 mg-C L^{-1}). From these

experiments, it was evident that increasing concentrations of IPA did not result in drastic changes in the observed photodegradation rate of niclosamide (**Figure S5**), in agreement with the efficiency calculations. Therefore, 25 mM IPA was selected as a conservative concentration and is expected to quench >99.6% of $^{\bullet}OH$ formed during sample irradiation. A 4 mM concentration of FFA and SA were selected to quench $^{1}O_2$ and ^{3}DOM, respectively. Although the selected 4 mM concentration of FFA is only sufficient to quench 62% of the $^{1}O_2$ formed, additional control experiments with higher concentrations of FFA led to deviations from pseudo-first-order kinetics (data not shown). The 4 mM concentration of sorbic acid is estimated to quench >95% of ^{3}DOM.

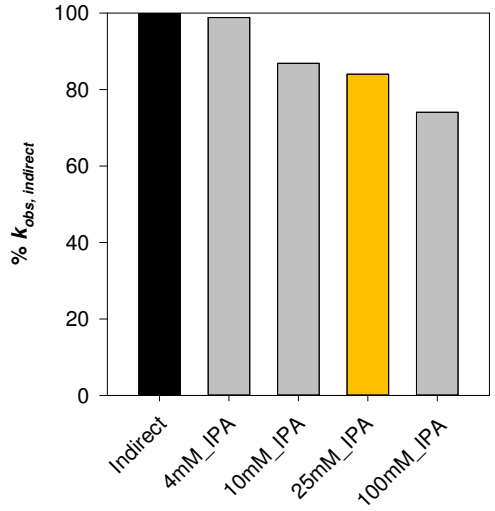

Figure S5. Impact of IPA concentration on the observed photodegradation rate of niclosamide in Milwaukee River Water. The black bar represents the observed indirect photodegradation rate of niclosamide in the absence of any quencher. The yellow bar represents the 25 mM concentration that was selected for subsequent probe/quencher experiments.

Section S5. Bimolecular rate constant determination.

Electron pulse radiolysis experiments and transient absorption detection were conducted at the Notre Dame Radiation Laboratory using previously described methods.[26–28] An 8 MeV Titan Beta model TBS-8/16-1S linear accelerator was utilized to determine the bimolecular rate

constants between $^{\bullet}OH$ or $CO_3^{-\bullet}$ and the two lampricides.[27] Absolute radical yields were determined using thiocyanate dosimetry, performed with nitrous oxide saturated (N_2O-saturated) solutions of 1.00×10^{-2} M potassium thiocyanate (KSCN) at a wavelength of 475 nm ($G\varepsilon = 5.2 \times 10^{-4}$ m^2 J^{-1}),[29] using doses of 3 – 5 Gy per 2 – 4 ns pulse. G is the radiation chemical yield (mol J^{-1}), ε is the molar absorption coefficient (m^2 mol^{-1}) and Gy is the absorbed dose (J kg^{-1}). Kinetic data were determined by averaging 12 to 15 replicate pulses in continuous flow mode.

Radiolysis of water produces a mixture of radical and molecular products according to the following equation:[23]

$$H_2O \rightarrow (0.28)^{\bullet}OH + (0.06)^{\bullet}H + (0.27)e^-_{aq} + (0.05)H_2 + (0.07)H_2O_2 + (0.27)H^+ \quad (S7)$$

The numbers in parentheses are the G-values (yields) in units of μmol J^{-1} of deposited energy. To examine the reactions of only $^{\bullet}OH$ with the two lampricides, solutions were pre-saturated with N_2O, which quantitatively converts the hydrated electrons (e^-_{aq}) and hydrogen atoms ($^{\bullet}H$) to $^{\bullet}OH$ according to the following reactions:[23]

$$e^-_{aq} + N_2O + (H_2O) \rightarrow N_2 + OH^- + {}^{\bullet}OH \qquad k_8 = 9.1 \times 10^9\ M^{-1}\ s^{-1} \quad (S8)$$

$$^{\bullet}H + N_2O \rightarrow N_2 + {}^{\bullet}OH \qquad k_9 = 2.1 \times 10^6\ M^{-1}\ s^{-1} \quad (S9)$$

In preparation for radiolysis, stock solutions containing TFM or niclosamide were prepared in 2.0 mM dibasic phosphate and adjusted to pH 8.0 (TFM) or 10.6 (niclosamide) using potassium hydroxide and/or perchloric acid. The reaction of $^{\bullet}OH$ with phosphate has a negligible contribution to the overall measured rate constant.[23]

Carbonate radical was generated through the reaction of $^{\bullet}OH$ with 0.10 M bicarbonate/ carbonate at a solution pH of 10.8 for both TFM and niclosamide according to the following equation:[23]

$$^{\bullet}OH + CO_3^{2-} \rightarrow OH^- + CO_3^{-\bullet} \qquad pK_a = 6.4,\ 10.3;\ k_{10} = 3.9 \times 10^8\ M^{-1}\ s^{-1} \quad (S10)$$

Under these experimental conditions, the reaction quantitatively generates carbonate radical ($CO_3^{-\bullet}$). All measurements were conducted at room temperature (22 ± 1 °C).

Hydroxyl radical reaction with TFM. The electron pulse radiolysis of a N_2O-saturated solution, containing an initial nominal TFM concentration of 261 μM, resulted in the transient difference spectrum shown in **Figure S6a** (inset). Typical pseudo-first-order growth kinetics were measured at the positive peak absorbance wavelength of 315 nm (**Figure S6a**). These absorbance data (Abs) were fit with a single exponential growth equation to determine the observed degradation rate (*k'*) at each concentration according to the following:

$$\text{Abs} = \text{Abs}^{\circ}(1-e^{-k't}) \quad \text{(S11)}$$

where Abs° is limiting absorbance observed over long time durations.

This analysis was replicated at four additional TFM concentrations (i.e., 0.58, 108, 145, and 204 μM). The fit determined for the exponential growth kinetics at each TFM concentration yields the second-order plot shown in **Figure S6b**. The slope of this line represents the absolute bimolecular rate constant for the reaction between $^{\bullet}OH$ and TFM (**Table S5**).

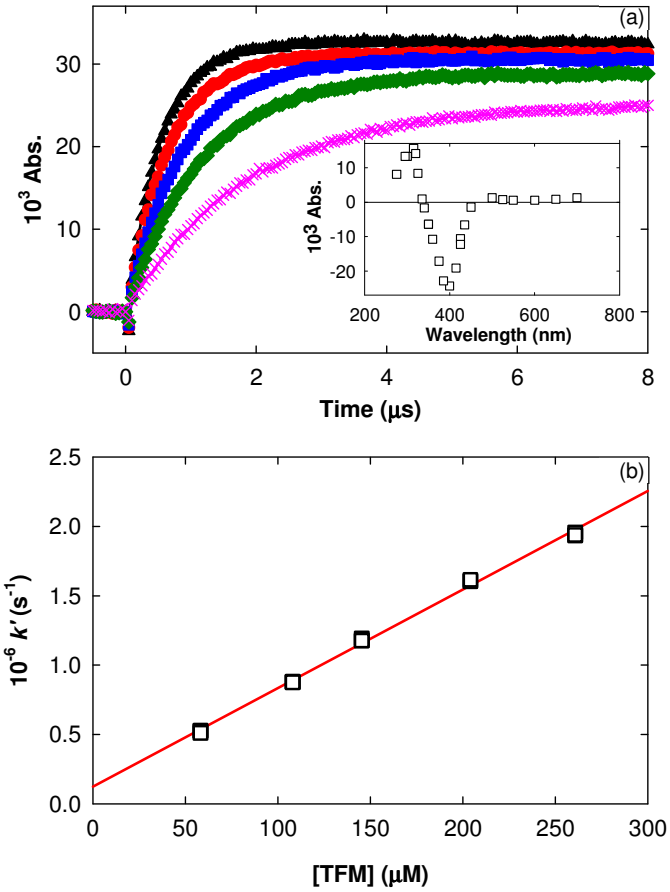

Figure S6. (a) Typical pseudo-first-order growth kinetics obtained at 315 nm for reaction of •OH with 261 (black triangles), 204 (red circles), 145 (blue squares), 108 (green diamonds) and 58 (pink x's) μM TFM at pH 8.0 and 22.1°C. Fitted lines correspond to exponential growth kinetics, with k' = (1.96 ± 0.01) × 10^6, (1.61 ± 0.04) × 10^5, (1.18 ± 0.01) × 10^6, (8.80 ± 0.04) × 10^5, and (5.27 ± 0.03) × 10^5 s^{-1}, respectively. Inset: Transient difference absorption spectrum obtained for the electron pulse radiolysis of 261 μM TFM in N_2O-saturated 2.0 mM phosphate buffered aqueous solution at pH 8.0 and 22.1°C. (b) Second-order rate constant determination from pseudo-first-order kinetics obtained from (a). Line corresponds to k = (7.11 ± 0.11) × 10^9 M^{-1} s^{-1}, r^2 = 0.997.

Table S5. Summary of bimolecular hydroxyl radical and carbonate radical rate constants for niclosamide and TFM.

Compound	•OH (M^{-1} s^{-1})	r^2	$CO_3^{-\bullet}$ (M^{-1} s^{-1})	r^2
Niclosamide	(7.48 ± 0.32) × 10^9	0.976	(6.19 ± 0.14) × 10^7	0.993
TFM	(7.11 ± 0.11) × 10^9	0.997	(1.17 ± 0.09) × 10^7	0.930
Mechanism	Monitor formation rate of oxidized species		Monitor degradation rate of carbonate species	

Hydroxyl radical reaction with niclosamide. Analogous •OH radical measurements were made for niclosamide. However, due to the low aqueous solubility of niclosamide (i.e., 15 – 45.9 µM; pH 7),[30,31] these kinetic rates were determined at pH 10.6 at concentrations at or below 50.7 µM. Kinetic data was collected at 435 nm for the reaction between •OH and niclosamide (18.4, 22.8, 31.2, 45.5, and 50.7 µM), resulting in the calculated second-order rate constant slightly faster than TFM presented in **Table S5** and **Figure S7**.

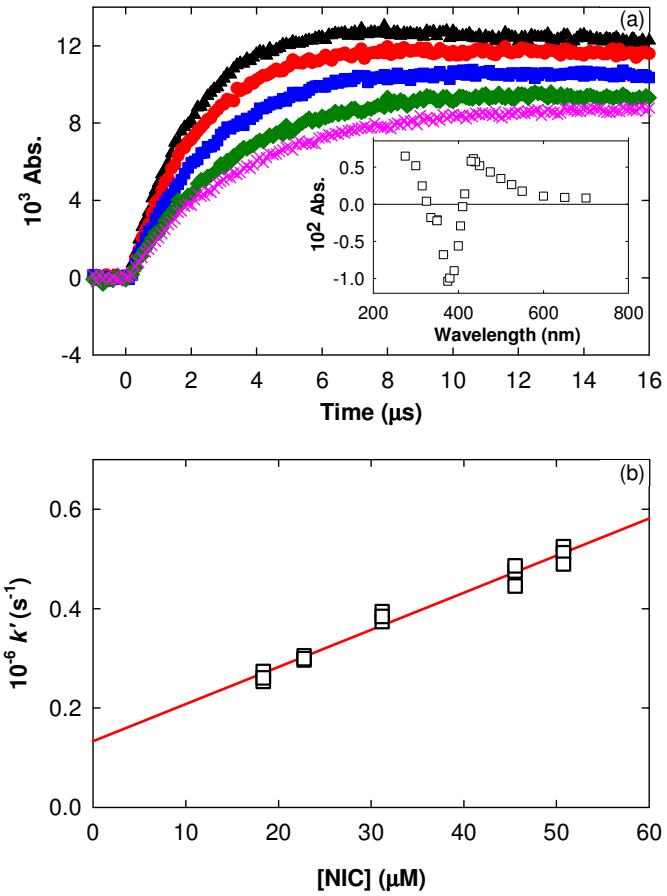

Figure S7. (a) Typical pseudo-first-order growth kinetics obtained at 435 nm for reaction of •OH with 50.7 (black triangles), 45.5 (red circles), 31.2 (blue squares), 22.8 (green diamonds) and 18.4 (pink x's) µM niclosamide at pH 10.4 and 22.1°C. Fitted lines correspond to exponential growth kinetics, with k' = (5.13 ± 0.05) × 10^5, (4.76 ± 0.08) × 10^5, (3.74 ± 0.07) × 10^5, (2.96 ± 0.23) × 10^5, and (2.53 ± 0.31) × 10^5 s^{-1}, respectively. Inset: Transient difference absorption spectrum obtained for the electron pulse radiolysis of 50.7 µM niclosamide in N_2O-saturated 2.0 mM phosphate buffered aqueous solution at pH 8.0 and 22.1°C. (b) Second-order rate constant determination from pseudo-first-order kinetics obtained from (a). Line corresponds to k = (7.48 ± 0.32) × 10^9 M^{-1} s^{-1}, r^2 = 0.976.

Carbonate radical reaction with TFM. The reaction of the carbonate radical with TFM generated a transient absorption difference spectrum, as shown in (**Figure S8a** (inset)). However, this radical also has a strong absorbance at 600 nm,[32] allowing direct monitoring of its reaction with TFM. The increased rate of $CO_3^{-\bullet}$ decay with TFM at 600 nm absorbance is shown in **Figure S8a**. This long timescale of the measured decay indicates that carbonate radical recombination:

$$CO_3^{-\bullet} + CO_3^{-\bullet} \rightarrow \text{products} \qquad 2k_{12} = 4.4 \times 10^6\ M^{-1}\ s^{-1} \qquad \text{(S12)}$$

competes with the reaction between TFM and $CO_3^{-\bullet}$ and thus the overall decay was found to be mixed-order.[23] By fitting a mixed order decay function to these absorbance data, the first-order component corresponding to the reaction between TFM and $CO_3^{-\bullet}$ was obtained, and is shown in the second-order plot (**Figure S8b**). These data result in a rate constant two orders of magnitude smaller than the reaction between TFM and $^{\bullet}OH$ (**Table S5**).

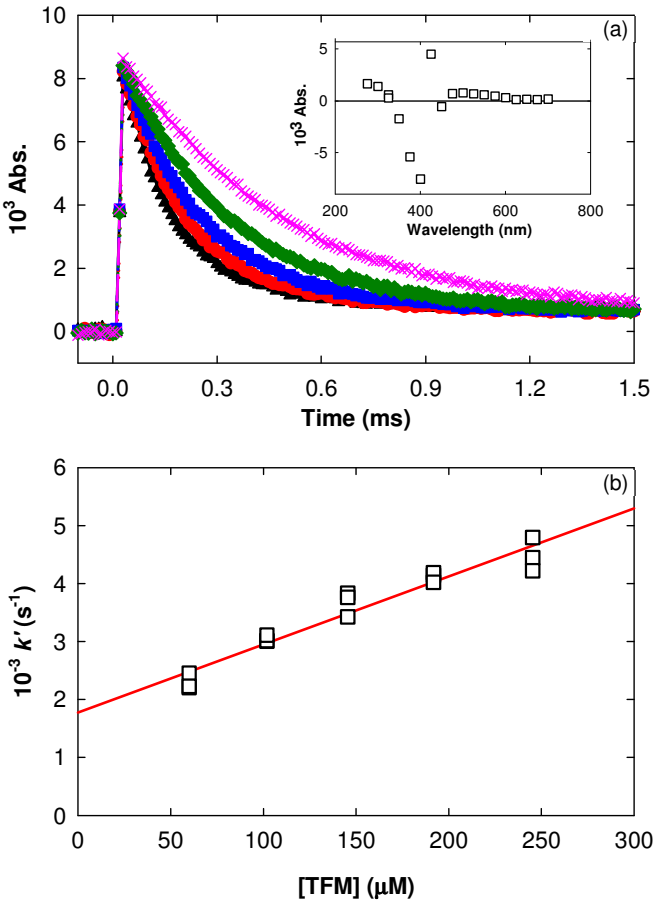

Figure S8. (a) Typical fit of mixed-order decay kinetics obtained at 600 nm for reaction of $CO_3^{-\bullet}$ with 245 (black triangles), 192 (red circles), 145 (blue squares), 102 (green diamonds) and 60 (pink x's) μM TFM at pH 10.9 and 22.1°C. Fitted lines correspond to exponential decay kinetics, with k' = (4.45 ± 0.12) × 10^3, (4.19 ± 0.09) × 10^3, (3.77 ± 0.0.06) × 10^3, (3.02 ± 0.0.06) × 10^3, and (2.45 ± 0.05) × 10^3 s^{-1}, respectively. Inset: Transient difference absorption spectrum obtained for the electron pulse radiolysis of 102 μM TFM and 0.10 M carbonate in N_2O-saturated aqueous solution at pH 10.9 and 22.1°C after all of the $CO_3^{-\bullet}$ had fully reacted with TFM. (b) Second-order rate constant determination from mixed-order decay kinetics obtained from (a). Line corresponds to k = (1.17 ± 0.09) × 10^7 M^{-1} s^{-1}, r^2 = 0.930.

Carbonate radical reaction with niclosamide. Analogous carbonate radical measurements were performed using niclosamide. A rate constant of (6.19 ± 0.14) × 10^7 M^{-1} s^{-1} was determined, which is slightly faster than the measured TFM carbonate biomolecular rate (**Table S5**, **Figure S9**). The more rapid rate of reaction with niclosamide implies that there may be additional reactive sites in this molecule compared to TFM.

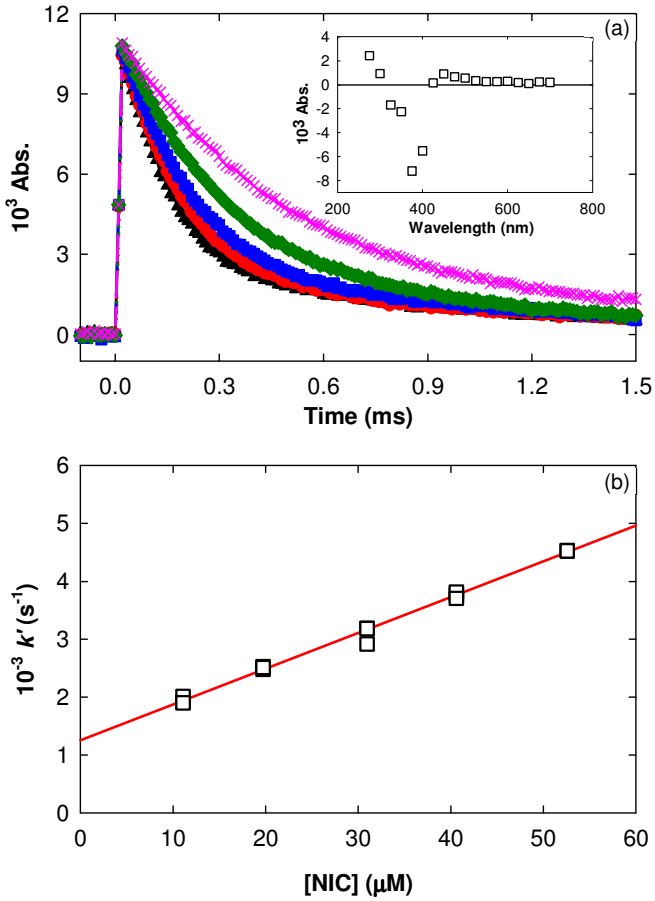

Figure S9. (a) Typical fit of mixed-order decay kinetics obtained at 600 nm for reaction of $CO_3^{-\bullet}$ with 52.6 (black triangles), 40.6 (red circles), 31.0 (blue squares), 19.7 (green diamonds) and 11.1 (pink x's) μM niclosamide at pH 10.9 and 22.1°C. Fitted lines correspond to exponential decay kinetics, with k' = (4.53 ± 0.70) × 10^3, (3.82 ± 0.80) × 10^3, (3.18 ± 0.70) × 10^3, (2.52 ± 0.20) × 10^3, and (2.01 ± 0.03) × 10^3 s^{-1}, respectively. Inset: Transient difference absorption spectrum obtained for the electron pulse radiolysis of 52.6 μM niclosamide and 0.10 M carbonate in N_2O-saturated aqueous solution at pH 10.9 and 22.1°C after all of the $CO_3^{-\bullet}$ had fully reacted with niclosamide. (b) Second-order rate constant determination from mixed-order decay kinetics obtained from (a). Line corresponds to k = (6.19 ± 0.14) × 10^7 M^{-1} s^{-1}, r^2 = 0.993.

Section S6. Analytical methods.

HPLC and LC-MS/MS analysis. High performance liquid chromatography (HPLC) and liquid chromatography-tandem mass spectrometry (LC-MS/MS) were used to analyze the organic samples collected during this study. HPLC analyses were performed with an Agilent 1260 instrument equipped with both a diode array detector (Model 1260 DAD; G4212B) and a fluorescence detector (Model 1260 FLD; G1321B). LC-MS/MS analyses were performed with an

Agilent 1260 HPLC equipped with a 6460-triple quadrupole mass spectrometer. The concentrations of niclosamide, TFM, the known organic photoproducts, and *para*-nitroanisole were quantified by HPLC and LC-MS/MS as described previously.[10] The loss of terephthalic acid and resulting formation of 4-hydroxy-terephthalic acid as a probe for $^{\bullet}OH$ formation were quantified by HPLC according to Method 1 below. The loss of furfuryl alcohol and 2,4,6-trimethylphenol were analyzed according to Methods 2 and 3, respectively.

Method 1: Quantification of TPA loss and hTPA formation:

Column:	Agilent Poroshell 120 Bonus RP (3.0 × 100 mm)
Guard column:	Agilent Bonus RP (3.0 × 5 mm)
Injection volume:	50 μL
Mobile phase:	A: 100 mM Formic Acid + 10% Methanol
	B: 100% ACN
Flowrate:	0.6 mL min^{-1}
Column temperature:	30^0C
Isocratic method:	50% A, 50% B
Method duration:	7.00 min

Target Analyte	**Wavelength (nm)**	**Excitation (nm)**	**Emission (nm)**	**Retention Time (min)**
TPA	254	--	--	1.31
hTPA	--	250	410	5.02

Method 2: Quantification of FFA:

Column:	Agilent Poroshell 120 EC-C18 (3.0 × 50 mm)
Guard column:	Agilent EC-C18 (3.0 × 5 mm)
Injection volume:	50 µL
Mobile phase:	A: 10 mM Ammonium Acetate + 10% Acetonitrile (ACN) adjusted to pH 7.5 (filtered through a 0.2 µm nylon filter) B: 100% ACN
Flowrate:	0.6 mL min^{-1}
Column temperature:	30^0C
Isocratic method:	100% A, 0% B
Method duration:	2.00 min, 0.5 min sample overlap

Target Analyte	Wavelength (nm)	Retention Time (min)
FFA	217	1.23

Method 3: Quantification of TMP:

Column:	Agilent Poroshell 120 EC-C18 (3.0 × 50 mm)
Guard column:	Agilent EC-C18 (3.0 × 5 mm)
Injection volume:	50 µL
Mobile phase:	A: 10 mM Ammonium Acetate + 10% Acetonitrile (ACN) adjusted to pH 7.5 (filtered through a 0.2 µm nylon filter) B: 100% ACN
Flowrate:	0.6 mL min^{-1}
Column temperature:	30^0C
Isocratic method:	50% A, 50% B
Method duration:	3.00 min + 0.5 min sample overlap

Target Analyte	Wavelength (nm)	Excitation (nm)	Emission (nm)	Retention Time (min)
TMP	277	230	325	1.35

Additional laboratory analysis. The chemical properties of the collected natural river water samples were analyzed in the laboratory (**Table S2**). Anions and cations were quantified by ion chromatography, while iron was determined using by inductively coupled plasma-optical emission spectrometry (ICP-OES; Perkin-Elmer 4300). Dissolved organic carbon measurements were made using a General Electric Sievers M5310C total organic analyzer, and UV-vis analyses were performed with a UV−vis spectrophotometer (Shimadzu UV-2401PC). Alkalinity was measured using a Mettler Toledo G-20 compact titrator.

Section S7. Inorganic mass balance and organic product formation.

The photodegradation of niclosamide and TFM leads to a combination of organic and inorganic products according to **Scheme S1**.

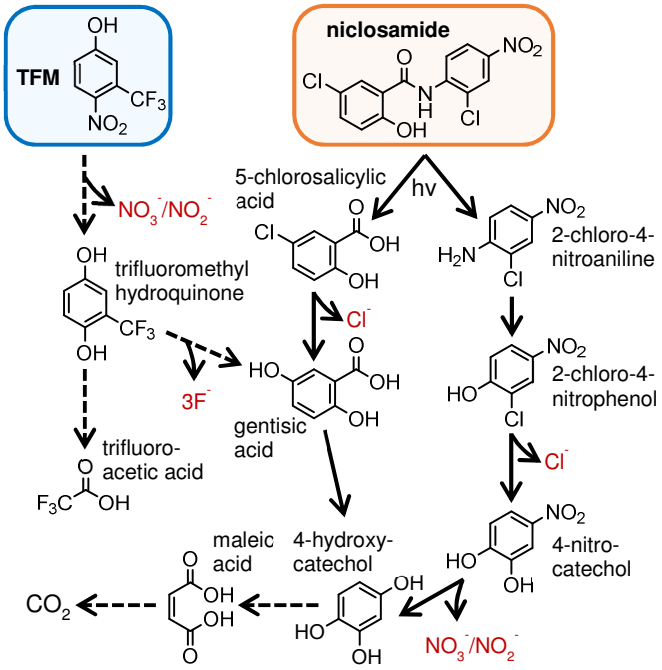

Scheme S1. Proposed photodegradation pathway for TFM and niclosamide adapted from McConville *et al.* 2016.[10] Segmented arrows represent a potential for multiple steps. Inorganic ions lost during irradiation are noted in red.

Inorganic mass balance calculations. Complete dehalogenation of 10 µM niclosamide and 10 µM TFM leads to the formation of 20 µM chloride (Cl^-) and 30 µM fluoride (F^-), respectively. Additionally, complete denitrogenation should lead to the formation of 10 µM nitrate/nitrite for both lampricides. Equation **S13** was used to calculate the material balance of the N-containing species for both molecules (i.e., TFM, nitrate, and nitrite for TFM and niclosamide, 2-chloro-4-nitroaniline, 2-chloro-4-nitrophenol, 4-nitrocatechol, nitrate, and nitrite for niclosamide). Equation **S14** was used to calculate the material balance for the F-containing species in TFM (i.e., TFM, trifluoroacetic acid, and fluoride) and equation **S15** was used to determine the

mass balance of the Cl-containing species in niclosamide (i.e., niclosamide, 5-chlorosalicylic acid, 2-chloro-4-nitroaniline, 2-chloro-4-nitrophenol, and chloride).

$$\text{Expected concentration} = C_t + (C_0 - C_t) \quad \text{(S13)}$$

$$\text{Expected concentration} = C_t + (C_0 - C_t)\cdot 3 \quad \text{(S14)}$$

$$\text{Expected concentration} = C_t + (C_0 - C_t)\cdot 2 \quad \text{(S15)}$$

where C_0 is the initial concentration of the relevant species and C_t is the concentration of those species at the time interval of interest.

To calculate the percent of inorganic conversion, the concentration of the specific inorganic species was divided by the amount of lampricide remaining in solution multiplied by the number of relevant inorganic ions (i.e., 2 = # chlorine atoms in niclosamide, 3 = # fluorine atoms in TFM, 1 = # nitro groups in TFM or niclosamide). The following calculation was performed to determine the percent conversion from TFM to F^-:

$$\%\ \text{Conversion to } F^- = \frac{[F^-]_t}{([TFM]_0 - [TFM]_t)\cdot 3}\cdot 100 \quad \text{(S16)}$$

where $[F^-]_t$ is the concentration of fluoride at any time t during the photolysis (μM), $[TFM]_0$ is the initial concentration of TFM (μM), $[TFM]_t$ is the concentration of TFM at any time *t* during the photolysis. Similarly, the following calculation was performed to determine the percent conversion from niclosamide or TFM to NO_3^-/NO_2^-:

$$\%\ \text{Conversion to } NO_3^-/NO_2^- = \frac{[NO_3^-]_t + [NO_2^-]_t}{([\text{lampricide}]_0 - [\text{lampricide}]_t)}\cdot 100 \quad \text{(S17)}$$

where lampricide represents either TFM or niclosamide. Finally, the percent conversion from niclosamide to chloride was calculated according to the following equation:

$$\%\ \text{Conversion to } Cl^- = \frac{[Cl^-]_t}{([NIC]_0 - [NIC]_t)\cdot 2}\cdot 100 \quad \text{(S18)}$$

Similarly, the percent conversion of niclosamide to 2-chloro-4-nitroaniline followed the outline for equation **S18**, though the Cl^- group was replaced with the concentration of 2-chloro-4-nitroaniline at time *t*.

Organic photoproduct direct and indirect photodegradation calculations. Organic photoproducts of niclosamide and TFM were irradiated in the presence and absence of DOM (pH 8, 450 W Xe-2 lamp). The following equation was employed to calculate the % rate increase observed during indirect photodegradation compared to direct photodegradation:

$$\% \text{ rate increase} = \frac{k_{obs,indirect} - k_{obs,direct}}{k_{obs,direct}} \cdot 100 \quad \text{(S19)}$$

Except for 5-chlorosalicylic acid, the photodegradation rates of all lampricide organic photoproducts were enhanced in solutions containing DOM.

The inorganic mass balance of F^- and NO_3^-/NO_2^- during TFM photodegradation in the presence and absence of DOM is presented in **Figure S10**. The formation of organic photoproducts during TFM photodegradation in the presence and absence of DOM is presented in **Figure S11**. The formation of inorganic and organic products during the direct and indirect photodegradation of niclosamide are presented in **Figures S12** and **S13**.

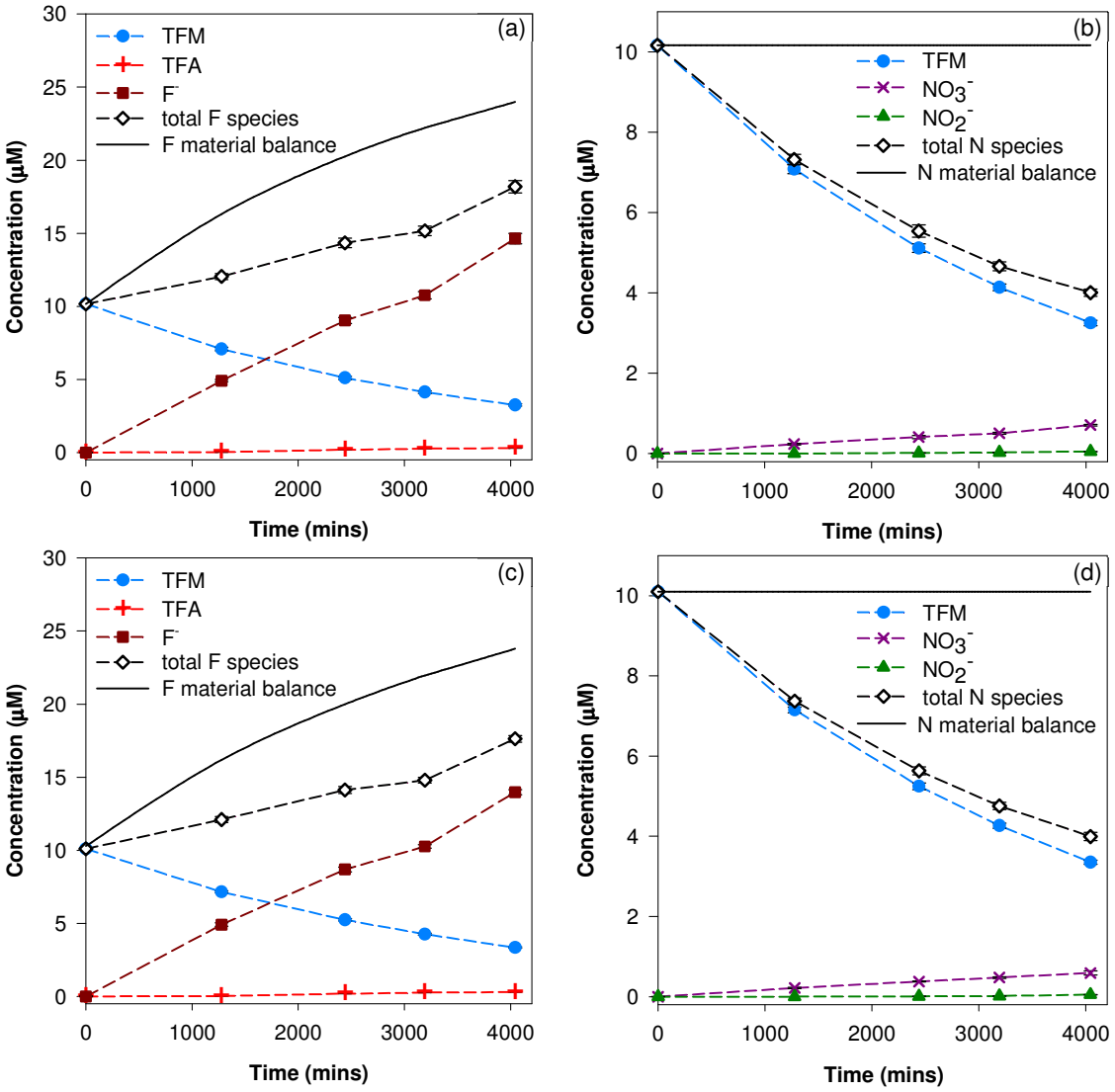

Figure S10. (a) TFM, trifluoroacetic acid (TFA), fluoride, and total F species and (b) TFM, nitrate, nitrite, and total N species generated during the direct photodegradation of TFM (pH 8). Total F species refers to the sum of [TFM], [TFA], and [F^-]. Total N species refers to the sum of [TFM], [NO_2^-], and [NO_3^-]. The solid lines represent the expected material balance of (a) [F^-] and (b) ([NO_3^-] + [NO_2^-]) assuming complete dehalogenation and denitrogenation of all organic compounds. The (c) F mass balance and (d) N mass balance for TFM photodegradation in the presence of 6.8 mg-C L^{-1} of Menominee River water.

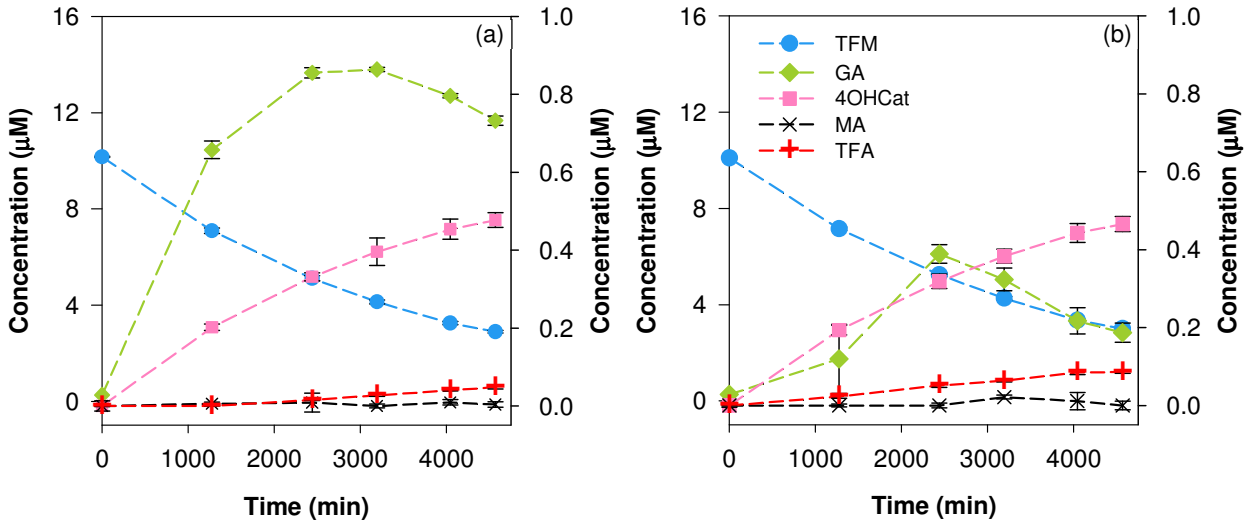

Figure S11. The loss of TFM in the (a) absence and (b) presence of DOM (Menominee River Water, pH 8, 6.8 mg-C L^{-1}) and the resulting formation of gentisic acid (GA), 4-hydroxycatechol (4OHCat), maleic acid (MA), and trifluoroacetic acid (TFA). TFM is plotted on the left y-axis, while all photoproducts are plotted on the right y-axis.

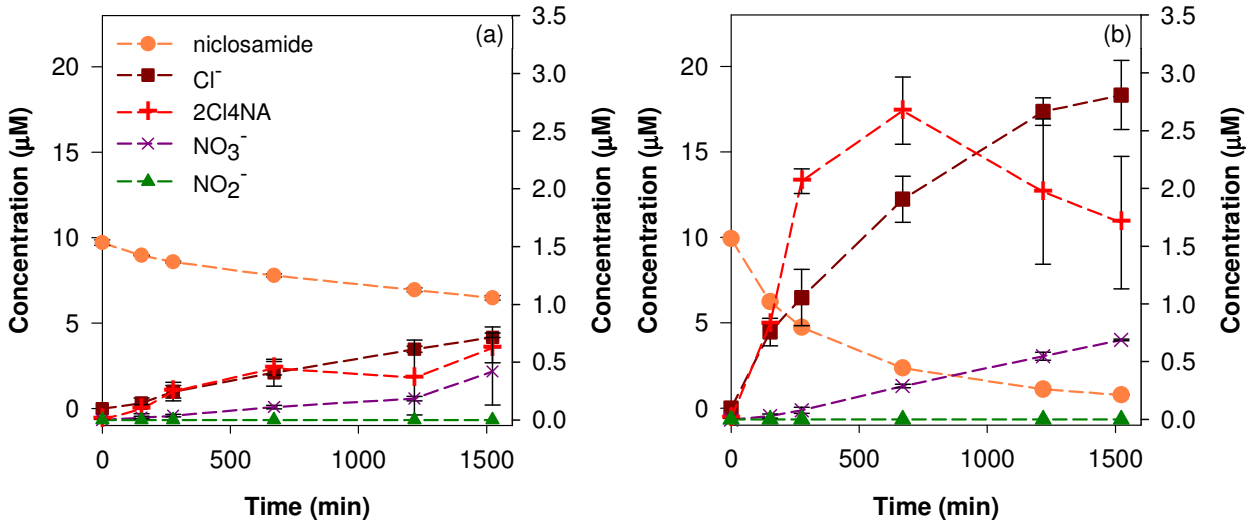

Figure S12. The loss of niclosamide in the (a) absence and (b) presence of DOM (Menominee River Water, pH 8, 6.8 mg-C L^{-1}) and the resulting formation of chloride, 2-chloro-4-nitroaniline (2Cl4NA), nitrate, and nitrite. Niclosamide and Cl^- are plotted on the left y-axis. 2Cl4NA, NO_3^-, and NO_2^- are plotted on the right y-axis.

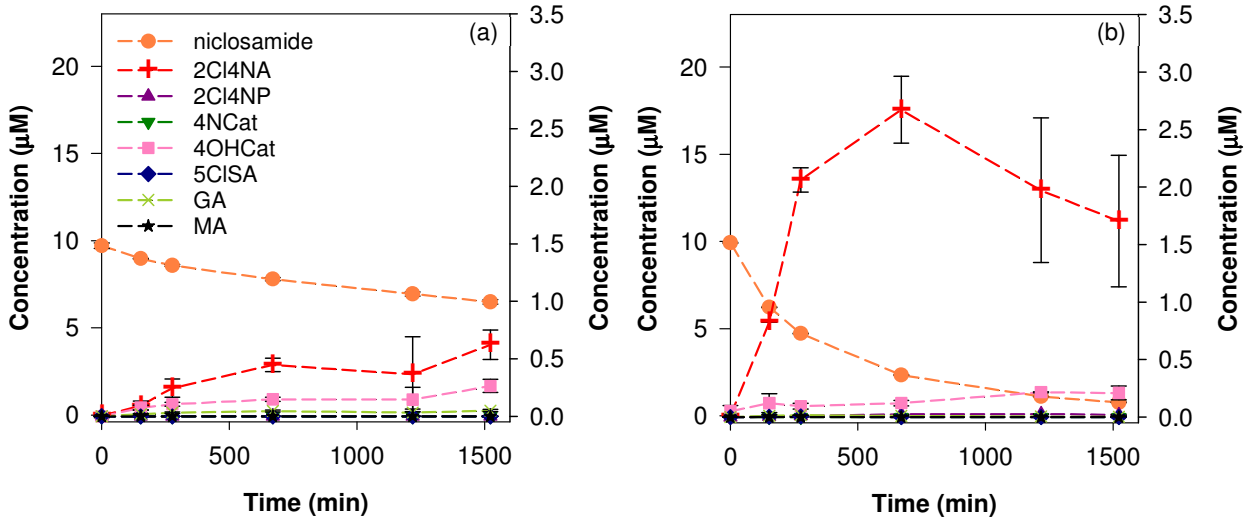

Figure S13. The loss of niclosamide in the (a) absence and (b) presence of DOM (Menominee River Water, pH 8, 6.8 mg-C L^{-1}) and the resulting formation of organic products. Niclosamide is plotted on the left y-axis. All products are plotted on the right y-axis.

Section S8. Quencher analysis.

A series of selective quenchers were added to solutions containing 10 μM niclosamide in natural river water samples. IPA was used to quench $^{\bullet}OH$ and limit the formation of $CO_3^{-\bullet}$, FFA was used to quench $^1O_2$, and sorbic acid was used to quench ^{3}DOM (**Figure S14**). Additional experiments to verify the influence of $^1O_2$ and ^{3}DOM on the observed photodegradation of niclosamide were conducted in D_2O (**Figure S15**) and in solutions sparged with nitrogen gas to reduce the concentration of molecular oxygen (**Figure S16**), respectively.

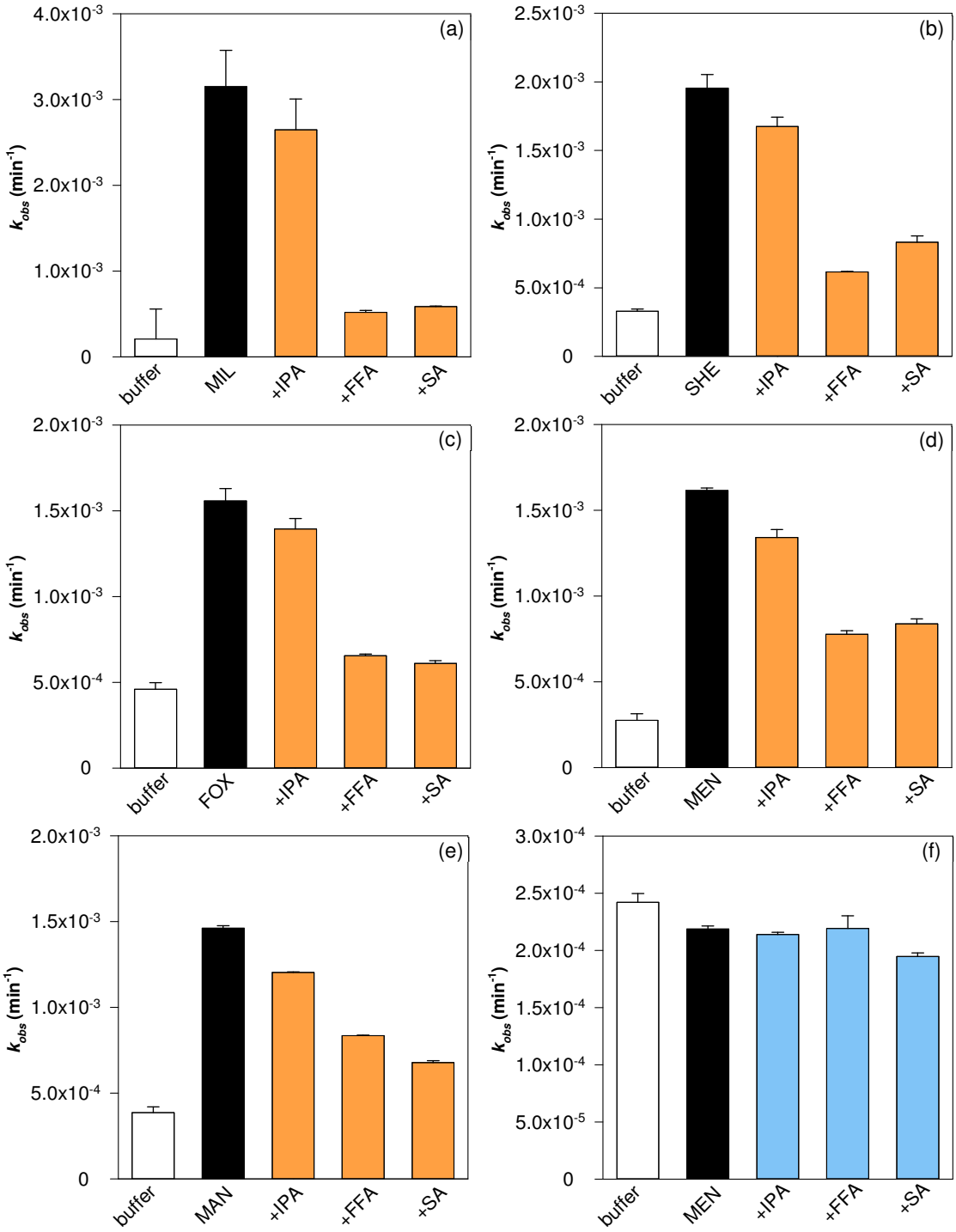

Figure S14. The observed photodegradation rates of (a – e) niclosamide and (f) TFM in the presence of 25 mM IPA, 4mM FFA, or 4 mM SA. Experiments were conducted at pH 8 in 5 mM borate buffer and (a) Milwaukee River water (MIL), (b) Sheboygan River water (SHE), (c) Fox River water (FOX), (d, f) Menominee River water (MEN), and (e) Manistique River water (MAN). All river water samples were adjusted to 6.8 mg-C L^{-1}.

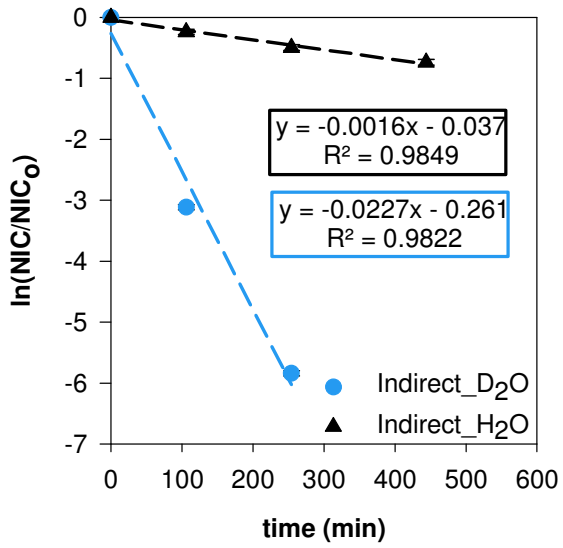

Figure S15. Indirect photodegradation rates (i.e., observed rates – direct photodegradation rates) of niclosamide in the presence of 6.8 mg-C L^{-1} SRFA in high purity water (H_2O) and in deuterium oxide (D_2O) at pH 8.00 and pD 8.40, respectively.

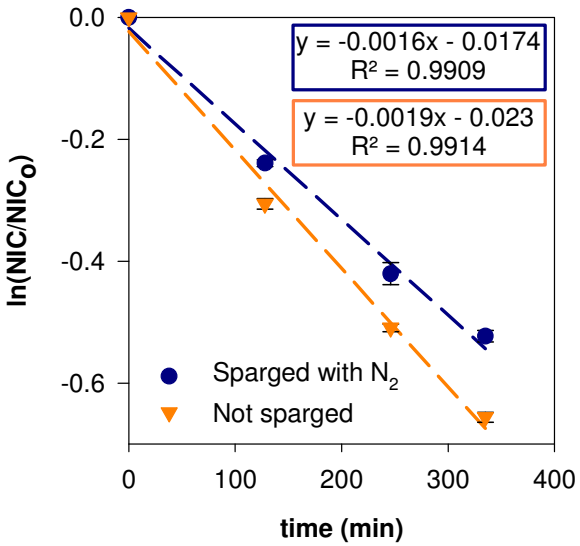

Figure S16. Observed photodegradation rates of niclosamide (6.8 mg-C L^{-1} Menominee River Water) in solutions sparged with nitrogen gas compared to samples in equilibrium with the atmosphere.

References.

1 D. K. Forsyth, C. M. Riseng, K. E. Wehrly, L. A. Mason, J. Gaiot, T. Hollenhorst, C. M. Johnston, C. Wyrzykowski, G. Annis, C. Castiglione, K. Todd, M. Robertson, D. M. Infante, L. Wang, J. E. McKenna and G. Whelan, *J. Am. Water Resour. Assoc.*, 2016, **52**, 1068–1088.

2 C. G. Homer, J. A. Dewitz, L. Yang, S. Jin, P. Danielson, G. Xian, J. Coulston, N. D. Herold, J. D. Wickham and K. Megown, *Photogramm. Eng. Remote Sens.*, 2015, **81**, 345–354.

3 L. Wang, C. M. Riseng, L. A. Mason, K. E. Wehrly, E. S. Rutherford, J. E. McKenna Jr., C. Castiglione, L. B. Johnson, D. M. Infante, S. Sowa, M. Robertson, J. Schaeffer, M. Khoury, J. Gaiot, T. Hollenhorst, C. Brooks and M. Coscarelli, *J. Gt. Lakes Res.*, 2015, **41**, 584–596.

4 S. F. Jane, L. A. Winslow, C. K. Remucal and K. C. Rose, *J. Geophys. Res. B.*, 2017, **122**, 546-561.

5 J. L. Weishaar, G. R. Aiken, B. A. Bergamaschi, M. S. Fram, R. Fujii and K. Mopper, *Environ. Sci. Technol.*, 2003, **37**, 4702–4708.

6 R. M. Cory and D. M. McKnight, *Environ. Sci. Technol.*, 2005, **39**, 8142–8149.

7 B. M. Peterson, A. M. McNally, R. M. Cory, J. D. Thoemke, J. B. Cotner and K. McNeill, *Environ. Sci. Technol.*, 2012, **46**, 7222–7229.

8 C. K. Remucal and K. McNeill, *Environ. Sci. Technol.*, 2011, **45**, 5230–5237.

9 J. R. Laszakovits, S. M. Berg, B. G. Anderson, J. E. O'Brien, K. H. Wammer and C. M. Sharpless, *Environ. Sci. Technol. Lett.*, 2016 **4**, 11-14.

10 M. B. McConville, T. D. Hubert and C. K. Remucal, *Environ. Sci. Technol.*, 2016, **50**, 9998–10006.

11 T. Zeng and W. A. Arnold, *Environ. Sci. Technol.*, 2012, **47**, 6735–6745.

12 W. R. Haag, J. Hoigné, E. Gassman and A. Braun, *Chemosphere*, 1984, **13**, 631–640.

13 D. E. Latch, B. L. Stender, J. L. Packer, W. A. Arnold and K. McNeill, *Environ. Sci. Technol.*, 2003, **37**, 3342–3350.

14 A. C. Maizel and C. K. Remucal, *Environ. Sci. Technol.*, 2017, **51**, 2113–2123.

15 E. Appiani, R. Ossola, D. E. Latch, P. R. Erickson and K. McNeill, *Environ. Sci. Process. Impacts*, 2017, **19**, 507–516.

16 S. Canonica, B. Hellrung and J. Wirz, *J. Phys. Chem. A*, 2000, **104**, 1226–1232.

17 A. L. Boreen, W. A. Arnold and K. McNeill, *Aquat. Sci.*, 2003, **65**, 320–341.

18 F. L. Rosario-Ortiz and S. Canonica, *Environ. Sci. Technol.*, 2016, **50**, 12532–12547.

19 S. E. Page, W. A. Arnold and K. McNeill, *J. Environ. Monit.*, 2010, **12**, 1658.

20 J. T. Jasper and D. L. Sedlak, *Environ. Sci. Technol.*, 2013, **47**, 10781–10790.

21 L. C. Bodhipaksha, C. M. Sharpless, Y.-P. Chin and A. A. MacKay, *Water Res.*, 2017, **110**, 170–179.

22 M. Minella, M. Rogora, D. Vione, V. Maurino and C. Minero, *Sci. Total Environ.*, 2011, **409**, 3463–3471.

23 G. V. Buxton, C. L. Greenstock, W. P. Helman and A. B. Ross, *J. Phys. Chem. Ref. Data*, 1988, **17**, 513–886

24 J. E. Grebel, J. J. Pignatello and W. A. Mitch, *Water Res.*, 2011, **45**, 6535–6544.

25 K. McNeill and S. Canonica, *Environ. Sci.: Processes Impacts*, 2016, **18**, 1381–1399.

26 W. Song, W. J. Cooper, S. P. Mezyk, J. Greaves and B. M. Peake, *Environ. Sci. Technol.*, 2008, **42**, 1256–1261.

27 K. Whitham, S. Lyons, R. Miller, D. Nett, P. Treas, A. Zante, R. W. Fessenden, M. D. Thomas and Y. Wang, *Proceedings of the 1995 Particle Accelerator Conference*, IEEE, 1995, vol. 1, pp. 131–133.

28 K. L. Swancutt, M. K. Dail, S. P. Mezyk and K. P. Ishida, *Chemosphere*, 2010, **81**, 339–344.

29 G. V. Buxton and C. R. Stuart, *J. Chem. Soc. Faraday Trans.*, 1995, **91**, 279–281.

30 F. Grifasi, M. R. Chierotti, K. Gaglioti, R. Gobetto, L. Maini, D. Braga, E. Dichiarante and M. Curzi, *Cryst. Growth Des.*, 2015, **15**, 1939–1948.

31 E. C. van Tonder, T. S. P. Maleka, W. Liebenberg, M. Song, D. E. Wurster and M. M. de Villiers, *Int. J. Pharm.*, 2004, **269**, 417–432.

32 G. L. Hug, *US Gov. Print. Office Wash. DC*, 1981, **NSRDS-NBS 69**, 1–167.